Verifying and Modeling the Polarizing Reflectance of Real-World Metallic Surfaces

Kai Berger, *Member, IEEE,* Andrea Weidlich, Alexander Wilkie, *Member, IEEE,*
Marcus Magnor, *Fellow, IEEE*

Abstract—In computer graphics, a large number of BRDF models have been introduced over the years. Some are purely appearance-based heuristics, while others are physically plausible. To achieve plausibility a lot of work has been done on measuring the actual reflectance of a wide range of material surfaces with BRDF models being fitted against these measurements. In this article, we present a systematic approach to *verify* the predictions of basic analytical BRDF models based on measurements of real-world samples. We show how to use ellipsometry as a way to verify both the actual polarizing effect as well as the overall reflectance behaviour of metallic surfaces.

1 Introduction

In order to generate convincingly rendered images of surface reflection appearances, computer graphics usually relies on phenomenologically motivated analytical BRDF models, e.g. Phong reflectance model [1]. In Believable Rendering applications, these intuitive models do not have to be physically accurate as long as the resulting image satisfies the expectations of the viewer.

This article focuses on Predictive Rendering, which relies on the BRDF models to make valid assumptions of the physical structure of the surface in order to correctly approximate the light transport in complex scenes. We identify the Fresnel reflectance and the Torrance-Sparrow model [2] as two well-known examples of so called physically plausible BRDF models. They predict the surface reflectance behaviour down to its reflective polarization properties.

In this article we attempt to verify the accuracy of such physically based models. We do this via ellipsometry. Ellipsometry is a measurement approach that can measure the polarization properties of light that is reflected from a surface. The reasons for this approach are twofold:

- In physics, ellipsometry is a standardized measurement process for reflectance behaviour of surfaces and objects. It even comes with off-the-shelve measurement equipment sufficient for our needs. So there is no need to engineer a suitable gonioreflectometer.
- For BRDF models that try to model reflectance polarization, we think it is best to measure their correctness based on the quality of reflective polarization prediction. Our main argument is, that measured polarization states can not be correctly predicted by the Fresnel formulae while normal reflectance values are incorrectly predicted by the Fresnel formulae at the same time. The correct prediction of polarization state implies reflectance value prediction.

We verified the polarization-capable BRDF models as follows:

- We collected a set of metallic surfaces since this sub-class is in our opinion the most useful and common type of surface in physically based rendering. The samples are commodity materials that can e.g. be obtained in a local hardware store, Sect. 3.2. We also included a gold and a silver coin in our set.
- We then measured the polarization properties with the ellipsometer, Sect. 3.4.
- We finally compared the measurements to the reflectances that we predict from the existing physically plausible BRDF models, Sect. 4.

2 Related work on BRDF models and ellipsometry

Phong [1] was the first to introduce an intuitive modeling of the light reflection process for surfaces. He constrained the model only to the principles of reciprocity and positivity. Ward and his colleagues [3] performed measurements of the reflection process and then fitted a suitable function to the numerical measurement results. A large database that consists only of the goniometric reflectance values for a huge variety of materials has been captured by Matusik and his colleagues [4], but they do not provide a model to explain the values. For physically based rendering, instead, we need a set of plausible BRDF models. These models assume an accurate representation of idealized surface patches. The most prominent model has been introduced by Torrance and Sparrow [2] back in 1967 in the physics community. This model has

been adapted by many researchers, e.g. Blinn [5] and Cook [6], to use different and neat microfacet models. However, these models have not been experimentally verified down to their polarization behaviour. Recent work in polarization-aware surface reflectometry has been published, but it rather presents measured data instead of validating existing models [7]. In our evaluation we focus on Torrance and Sparrow's BRDF-model as a representative of physically plausible models and we vary over different microfacet models. Also, we compare our real-world measurements to the Fresnel-Equations. We seek to verify physically plausible models with the equations of Ellipsometry. The equations, as we use them, were derived by Paul Drude, Fig. 1 (top right) in 1887. Around 1901, an early instrument was imaged by Drude (top left). However, a first ellipsometric measurement instrument was completed by Jules-Celestin Jamin and their work was published in 1847. Back then, it consisted of two telescopes with attached linear polarizers. The image was formed at the naked human eye. The name ellipsometer, however, was first introduced February 1945 by Alexandre Rother in Review of Scientifc Instruments, Vol. 16. Until the 1940s ellipsometry did not take wavelength-dependency into account. The technique was to rotate the analyzer until an intensity minimum, ideally zero intensity, was reached (Null ellipsometry). However, this method was very time-consuming. A measurement of a surface patch took about an hour. Therefor the photometric ellipsometer configuration emerged. The polarizer is fixed at $45°$ and a retarder is optionally placed inside the beam. The reflected light is always elliptically polarized, so that analyzer simply has to rotate continuously and the intensity of the resulting beam is a sinusoid over time. After Fourier analysis Ψ and Δ can be retrieved. Our ellipsometer is based on the spectroscopic ellipsometer configuration which was first developed in 1975 by Aspnes and his colleagues. The emitted light is produced by a white light source, and the retrieved light passes a monochromator, Fig. 1 (bottom). Recent approaches in the area of digizing cultural heritage succeed in employing spectroscopic ellipsometry as well [8], [9]. They however restricted themselves to reconstructing artifacts made of alloys, such as bronze, and copper.

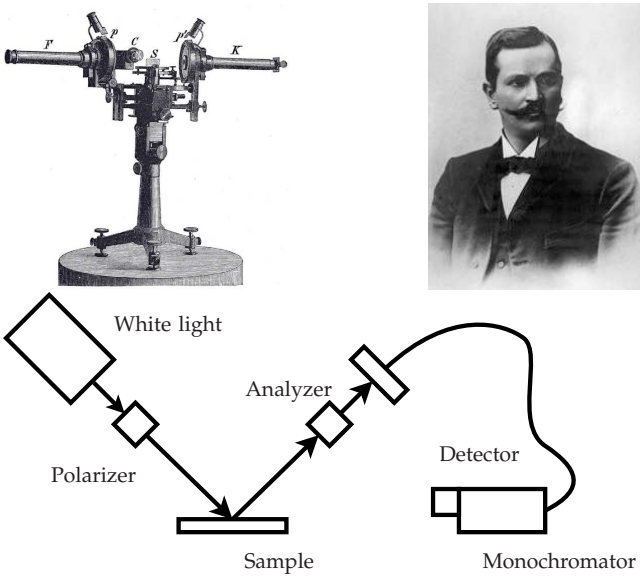

Fig. 1: The earliest instrument (top left, reproduced from http://www.bam.de/en/microsites/ake/ellipsometrie.htm) to measure the reflection polarization for materials has been introduced by Paul Drude (top right,*1863 in Braunschweig †1906 in Berlin, reproduced from Wikipedia, Public Domain). However, it was not named an ellipsometer before 1945. A surface S is placed between the telescopes F and K, both attached to polarizers p and p'. The image was formed in the human eye. The SENTECH ellipsometer implements the spectroscopic ellipsometry technique as depicted at the bottom

3 Our Measurement Approach

3.1 Ellipsometry as reflectance measurement

Usually in computer graphics reflected light is represented as a triplet of RGB values and measured with a gonioreflectometer for varying incident and exitant angles.

We would store the measured intensity values in lookup tables [10] or we would approximate them with BRDF models that can be quickly evaluated on the GPU in real-time.

However, in our article we compute BRDF values from measured polarising behaviors. We reason this by providing *both* a valid statement about the polarising behaviour *and* a valid reflectance value for a particular incident angle and wavelength.

We do so because we do not consider light as a scalar value. Instead, we think of it as an electromagnetic wave traveling through space with a field behaviour in space and time. The wave is described by its parallel (p-plane) and perpendicular (s-plane) components. In Fig. 2 a typical reflected electromagnetic light wave is shown. During the reflection it is exposed to attenuation and phase shift.

The incident wave $\vec{E_\lambda}$ with a wavelength λ is reflected from the surface to become $\vec{R_\lambda}$ and is exposed to changes in phase and amplitude. This results in different field values in the reflected wave $\vec{R_\lambda}$. We know that these changes directly relate to the parallel r_p and perpendicular r_s reflectance values from the well-known Fresnel equations and affect the overall perceived intensity as we will show in Sect. 3.2.

3.2 The Fundamental Equation of Ellipsometry

We first measure the polarization state of the reflected light for a varying wavelength λ with an ellipsometer.

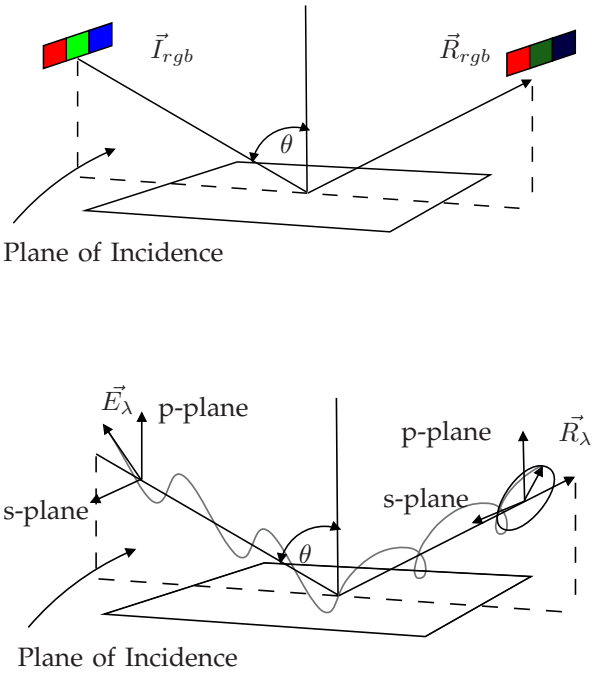

Fig. 2: In computer graphics, reflected light is usually considered as a scalar or as an RGB-triplet (top). In this article, instead, we consider the spectrum of light waves $\vec{R_\lambda}$, that are attenuated and shifted in phase. We measure the wavelength-dependent ratio of parallel and perpendicular reflectance values of a surface with an ellipsometer. The combination of both reflectance values defines the perceived intensity of the reflected light (bottom).

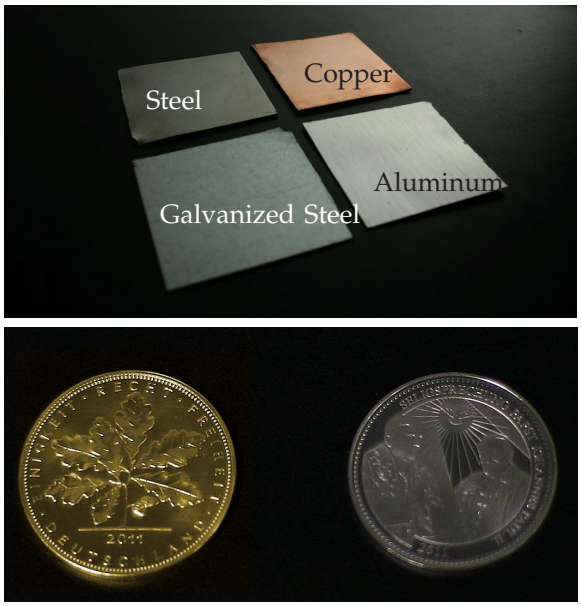

Fig. 3: We evaluated the following examples (top): steel, copper, galvanized steel and anodized aluminium (E6). We also evaluated a gold (bottom left) and a silver coin (bottom right).

The state is characterized by the parameters Ψ and Δ. We can think of Ψ and Δ as the amplitude attenuation and phase shift induced to the reflected light wave, Sect. 3.1. From these values we want to compute the ratio of parallel reflectance r_p and perpendicular reflectance r_s values against which we compare the estimated reflectance values of existing models.

We use the *Fundamental Equation of Ellipsometry* for this conversion. This equation states that

$$\rho = tan(\Psi)e^{i\Delta} = \frac{r_p}{r_s} \tag{1}$$

with ρ, r_p and $r_s \in \mathbb{C}$. A thorough derivation of the equation can be found in [11] pp. 529 - 531. We provide a short version in the Appendix. As already mentioned, our ellipsometer can only measure Ψ and Δ for given angle of inclination and a given wavelength. Thus we have to compute $\rho_{data} = tan(\Psi)e^{i\Delta}$ from the measured Ψ and Δ values, using Eqn. 1. We then can compare the models to these values.

We only have to derive $r_{p_{model}}$ and $r_{s_{model}}$ for a physically plausible BRDF model $model$ and let $\rho_{model} = \frac{r_{p_{model}}}{r_{s_{model}}}$.

Finally, we perform a fitting of $|\rho_{model}|^2$ for the model parameters to the values $|\rho_{data}|^2$ that we just computed from the measured Ψ and Δ values using the Fundamental Equation of Ellipsometry.

3.3 Measured Samples

For the verification of the physically plausible BRDF models with our ellipsometer, we decided to choose the following commodity metals: copper, steel, aluminum, and galvanized steel, Fig. 3. When we decided for aluminum we were faced with two different kinds of products: commodity aluminum foil and anodized aluminium (E6) that is usually sold in hardware stores. We therefore performed a measurement for both types. We also evaluated a gold and a silver coin with a purity of $99,9\%$. Note, that the gold and silver sample were not cleaned or coated with a protector film before measurement. They were measured directly after being produced in the coining machine.

3.4 Measurement Device

We performed the ellipsometric measurement, i.e. the measurement of Ψ and Δ for varying wavelength λ, with an ellipsometer as depicted in Fig. 4. For our purposes, we used the SE-800 ellipsometer from SENTECH. The ellipsometer captures a spectral range from $246nm$ to $866nm$ and operates as a Step Scan Polarizer. The light is produced by a stabilized noise-reduced $75W$ Xe lamp. In two cycles the ellipsometer

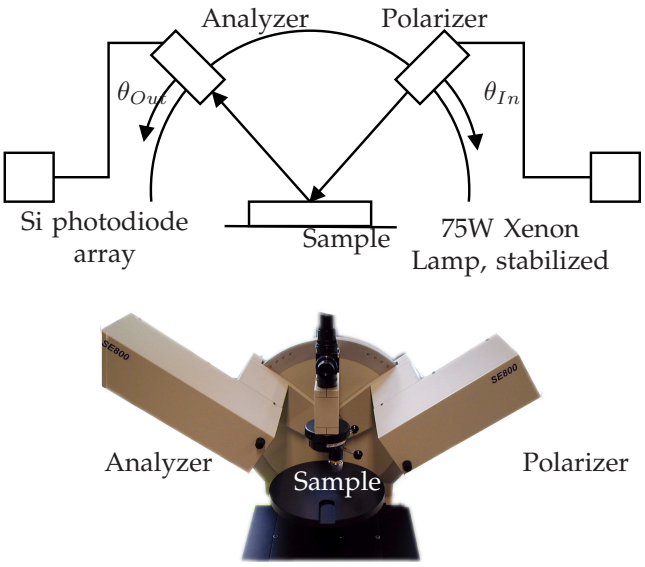

Fig. 4: Top: Schematic depiction of our setup. Bottom: SE-800 ellipsometer from SENTECH.

measures the Ψ and Δ values. The measurement inaccuracy of the ellipsometer is in the range $d\Psi = \pm 0.05°$ and $d\Delta = \pm 0.1°$.

We evaluate the polarization parameters $\Psi(\lambda)$,$\Delta(\lambda)$ for a finite set of angles θ, by utilizing its goniometer. We limit the measurements to the following angles of incidence $45°$, $50°$, $60°$, $70°$, $75°$ and $80°$. The incident and exitant angle are identical.

4 Results

We measured the four metallic surface patches and the two silver coins. We evaluated the data in the VIS range, i.e. $380 - 750nm$. A typical plot for Ψ and Δ is depicted in Fig. 5 (left). Then we computed their reflectance ratios for varying wavelength using Eqn.1, Sect. 3.2. We found that the computed values fit the values predicted in literature, Fig. 5 (middle, right). Finally, we fitted the physically-based BRDF models, i.e. the Torrance-Sparrow model with different distribution functions, to get a statement about the goodness of their applicability to real-world surface materials, Table 1.

4.1 Results - Example 1: Copper

For the copper surface we will exemplary describe the fitting of physically based rendering models.

From the measured Ψ and Δ values, Fig. 5 (left), we computed the squared reflectance ratio $|\rho_{data}|^2 = |tan(\Psi)e^{i\Delta}|^2$ and compared it to the estimated reflectance ratio from literature [12], Fig. 5 (middle).

Then, we performed the fitting. We examined the Fresnel-terms

$$Fr_\perp = \frac{(a - cos\theta)^2 + b^2)}{(a + cos\theta)^2 + b^2)} \tag{2}$$

$$Fr_\parallel = Fr_\perp \frac{(a - sin\theta)^2 + b^2)}{(a + sin\theta tan\theta)^2 + b^2)} \tag{3}$$

with

$$a^2 = \frac{1}{2}(\sqrt{n^2 - k^2 - sin^2\theta + 4n^2k^2}) + (n^2 - k^2 - sin^2\theta)$$

$$b^2 = \frac{1}{2}(\sqrt{n^2 - k^2 - sin^2\theta + 4n^2k^2}) - (n^2 - k^2 - sin^2\theta)$$

and plotted $|\rho_{data}|^2 = |tan(\Psi)e^{i\Delta}|^2$ against $|\frac{Fr_\parallel}{Fr_\perp}|^2$. We also examined the Torrance-Sparrow [13] model with different microfacet distributions:

$$r_i = \frac{1}{4cos(\theta_o)cos(\theta_i)} * Fr_i * G(\theta_o, \theta_i) * D_n \tag{4}$$

with geometric term G for shadowing of illuminating rays and masking of absorbed viewing rays and where $i \in \{\perp, \parallel\}$. In our measurement setup θ_o equals θ_i and in the fitting procedure we let G constant and n vary over the following microfacet distributions:

- Blinn-Phong [5]
- Gaussian [13]
- Beckmann [14]
- Trowbridge and Reitz [15]

Their formulae are given in the appendix. We used Mathematica's *NonLinearModelFit* and provided an initial guess to the complex refractive index values (n,k) of copper and the surface roughness parameter β in the microfacet distribution for the given wavelength λ. In Fig. 5 (right), the fitting results for the refractive index n and absorption coefficient k of copper in the VIS-range are plotted against the predicted values by the literature [12]. Note, that the plot for the fitted absorption coefficient k is slightly exceeded by literature values. In Table 1, first column lists the fitting results for copper in detail. We could perform the fitting for steel and galvanized steel in the same way, the results are also shown in Table 1.

4.2 Results - Example 2: Aluminum

For the anodized aluminium (E6) patch we observed an interesting behaviour in the measured data. The plots for Ψ and Δ oscillate over the measured spectrum, Fig. 6. Thus the computed reflectance ratio oscillates over the measured range, Fig. 6 (top right). A fitting as in Example 1 could not be performed adhoc. We figure, this is due to the Al_2O_3 oxide layer that is situated on top of the aluminum surface. This can be accounted for by assuming a thin layer of $3\mu m$ on top of the substrate with known complex refractive index. For the substrate we assumed the index $n = 0.11945$ and $k = 2.26534$ for $\lambda = 550nm$. The thin film assumed as porous aluminum oxide.

When we examined aluminum foil with a much thinner oxide layer, instead, we found out, that the computed reflectance ratio values approximately fit to the predicted behaviour, Fig. 6 (bottom right). Table 1, fourth column lists the different fitting results for aluminum foil for a wavelength of $\lambda = 516nm$.

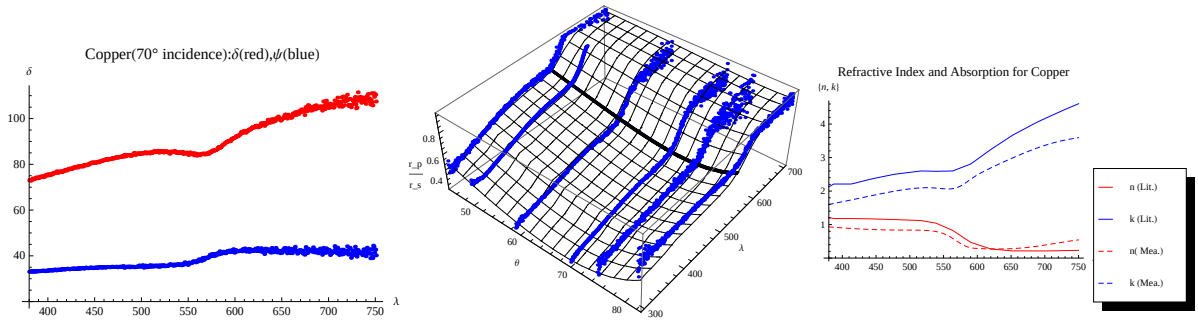

Fig. 5: The ellipsometric measurement data for copper (left) in the VIS-range. The blue plot shows the Ψ, the red plot shows the Δ values (in degree) for an inclination $\theta = 75°$. The reflectance ratios computed with Eqn.1 fit to the predicted behaviour by the Fresnel equations (middle). This plot visualizes the reflectance ratios $\frac{r_p}{r_s}$ computed with Eqn.1 (blue dots) for varying inclination θ (in degree) and a wavelength λ (in nm). It matches the reflectance ratios $\frac{Fr_{\parallel}}{Fr_{\perp}}$ of copper as stated in the literature [12] (black grid). In the right plot An exemplary fit of the refractive index and absorption coefficient to the measured data is plotted against the refractive index and absorption coefficient in the literature [12] for the VIS-range.

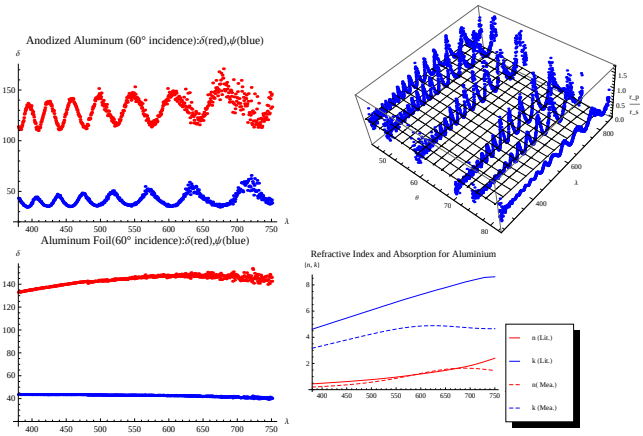

Fig. 6: Anodized aluminum (E6) shows an oscillating behaviour in the VIS-range (top left). The blue plot shows the Ψ, the red plot shows the Δ values (in degree) for an inclination $\theta = 60°$. The reflectance ratios computed with Eqn.1 do not fit to the predicted behaviour by the Fresnel equations (top right). This plot visualizes the reflectance ratios $\frac{r_p}{r_s}$ computed with Eqn.1 (blue dots) for varying inclination θ (in degree) and a wavelength λ (in nm). It does not match the reflectance ratios $\frac{Fr_{\parallel}}{Fr_{\perp}}$ of aluminum as stated in the literature [12] (black grid). however, aluminum foil shows the expected behaviour in the measured range (bottom row).

4.3 Results - Example 3: Gold and silver coin

Like in Example 1 , we could fit the measurement data to the model. From the measured Ψ and Δ values for the gold coin, Fig. 7 (left), we computed the reflectance ratio $|\rho_{data}|^2 = |tan(\Psi)e^{i\Delta}|^2$ and compared it to the reflectance ratio in literature [12], Fig. 7 (middle). We found that the measured data fit very accurately to the predicted values in the literature. As in Example 1, we could fit the refractive index and absorption coefficient to the measured data points, Fig. 7 (right). We could also fit the refractive index and absorption coefficient for the silver coin, Fig. 8 (right). Note, that the plot for the fitted absorption coefficient k is a bit exceeded by literature values, while the plot for the fitted refractive index n slightly exceeds by literature values. Interestingly, we found that this holds only for non-polished surface spots. If the coin is proof (PR, PF) then there is a noticeable drop in the reflectance ratio for wavelengths beyond $470nm$ which is not explained by the literature. Table 1, fifth and sixth columns show the different fitting results for gold for a wavelength of $\lambda = 516nm$ and silver for a wavelength of $\lambda = 495nm$.

4.4 Results - Rendering

At last, We compared the rendering output generated with the fitted refractive index and absorption coefficient to the renderings generated with the literature values. We used the state-of-the-art renderer PBRT 2.0 [16], and modeled a scene showcasing a halfsphere in the middle of the Uffizi scene. We set its surface roughness $\beta = 0.0001$ to increase the reflection of the surrounding scene. All renderings are shown in Fig. 9. The first row shows the sphere's coating with the n, k values fitted to our ellipsometric measurement data (cf. Fig. 5 (right),8 (right),7 (right)). The second row shows the sphere's coating as stated in the literature [12]. Note, that the renderings were tonemapped [17] for display in the paper. In the third row the absolute per pixel intensity difference is plotted on a logarithmic scale. We evaluated copper, silver, gold, aluminum and zinc-covered steel. The images rendered with a gold coating show the least differences, the images rendered with an aluminum and a silver coating show the most noticeable difference. However, all differences remain subtle, i.e. the coatings computed with the ellipsometric measure-

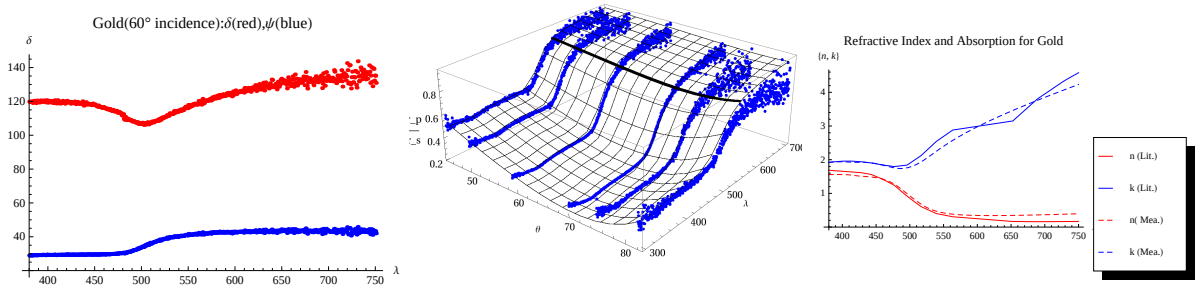

Fig. 7: Gold shows a stable behaviour in the VIS-range(left). The blue plot shows the Ψ, the red plot shows the Δ values (in degree) for an inclination $\theta = 60°$. The reflectance ratios computed with Eqn.1 match the predicted behaviour by the Fresnel equations very accurately (middle). In the right plot An exemplary fit of the refractive index and absorption coefficient to the measured data is plotted against the refractive index and absorption coefficient in the literature [12] for the VIS-range.

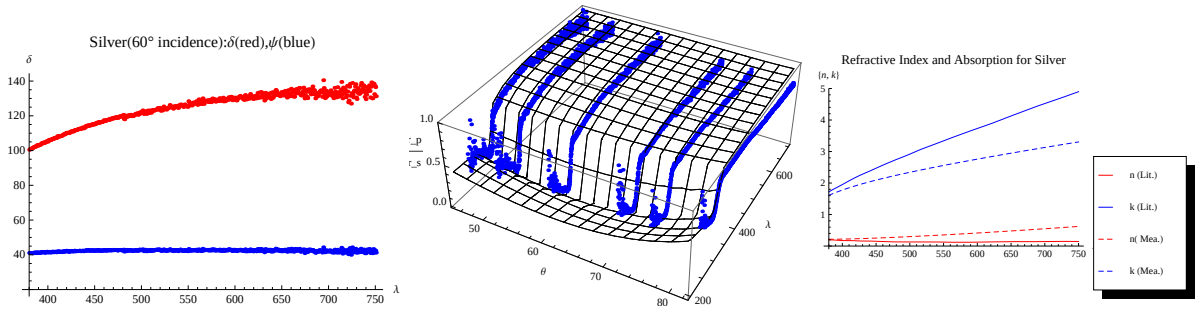

Fig. 8: Silver shows a stable behaviour in the VIS-range (left). The blue plot shows the Ψ, the red plot shows the Δ values (in degree) for an inclination $\theta = 60°$. The reflectance ratios computed with Eqn.1 match the predicted behaviour by the Fresnel equations (middle). In the right plot An exemplary fit of the refractive index and absorption coefficient to the measured data is plotted against the refractive index and absorption coefficient in the literature [12] for the VIS-range.

ment data from real-world surfaces fit visually to the coatings predicted from the literature [12].

5 Conclusion

We introduced the ellipsometer, traditionally a non-destructive and contactless tool with very general applications in biology, semiconductor physics or microelectronics, as a BRDF verification method in computer graphics. We could verify the predicted reflectance values of BRDFs which are considered as physically plausible for a different set of metals including gold and silver. This is especially important in Predictive Rendering. By using an ellipsometer we could provide real-world measurement down to the level of polarization behaviour. Interestingly, we found that anodized aluminum showed a different behaviour at the first glance. The reflectance ratio oscillates for increasing wavelength. This can be accounted for by assuming a layered model including an oxide layer. Finally, we presented rendered images to show that the coatings computed with the ellipsometric measurement data fit visually to the coatings predicted from the literature. We conclude that we could justify the existence of physically-based models in Predictive Rendering.

Nomenclature

β	Surface roughness expressed as Root Mean Square Slope. $\beta \in (0°..90°)$
Δ	Phase shift of light induced by surface reflectance. Wavelength-dependent.
λ	Wavelength of Light.
Ψ,$tan\Psi$	Attenuation of light induced by surface reflectance. Wavelength-dependent.
$\rho_{model,data}$	Complex reflectance ratio. Estimated from a BRDF model, or computed from Ψ and Δ. Wavelength-dependent. $\rho \in \mathbb{C}$.
θ	Inclination angle w.r.t the surface normal. $\theta \in (0°..90°)$. In this article the incident angle θ_i equals the exitant angle θ_o.
D_n	Microfacet Distribution function. In this article n varies over Blinn-Phong [5], Gaussian [13], Beckmann [14] and Trowbridge and Reitz [15].
$Fr_{\parallel,\perp}$	Fresnel reflection terms form parrallel and perpendicular polarized light. Wavelength-dependent.

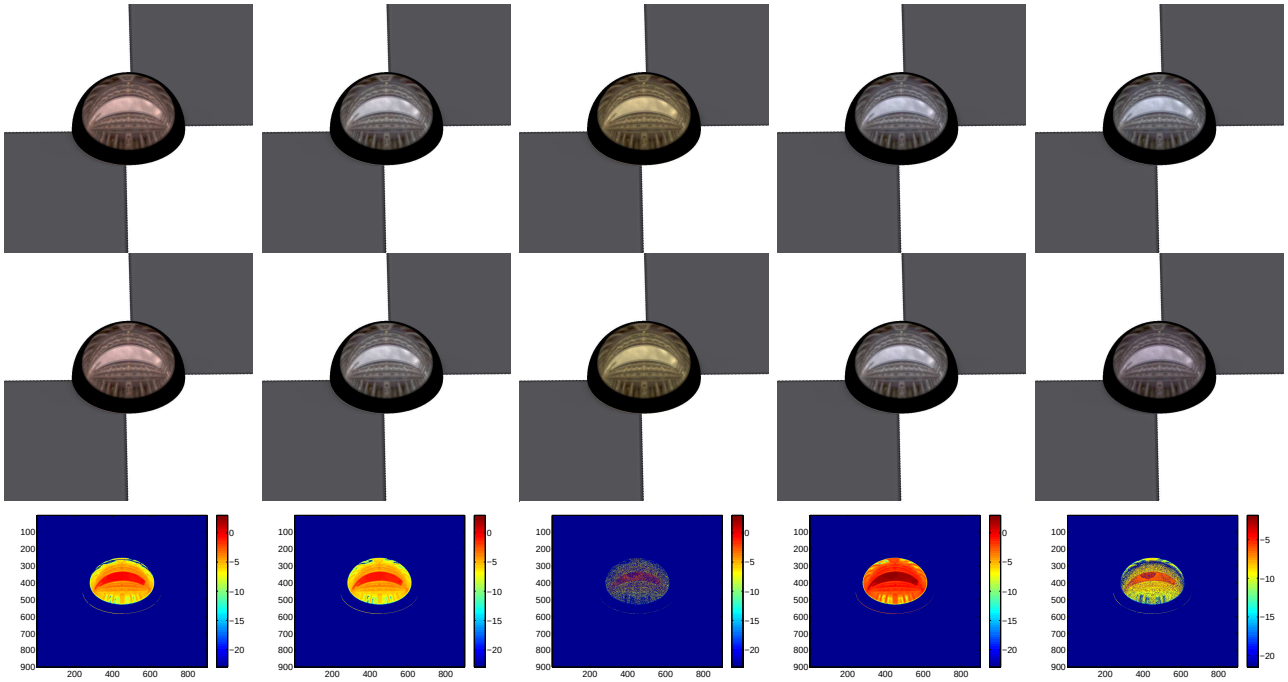

Fig. 9: Renderings based on our measurements (top) and literature models (middle) show subtle differences (bottom). The first row shows a coating with fitted n, k values to our ellipsometric measurement data. The second row shows the coating as stated in the literature [12]. The third row shows the per pixel difference on log-scale. From left to right: copper, silver, gold,aluminum,zinc. The images were rendered with PBRT [16] and tonemapped with Durand's algorithm [17] for display.

k Extinction coefficient of the surface material. Wavelength-dependent.

n Refractive index of the surface material. Wavelength-dependent.

r_p Parallel (p) field component of the reflected light wave w.r.t the plane of incidence. $r_p \in \mathbb{C}$.

r_s Perpendicular (s = German senkrecht) field component of the reflected light wave w.r.t the plane of incidence. $r_s \in \mathbb{C}$.

Appendix - Derivation of the fundamental equation of ellipsometry

Here, we provide for a short derivation of the fundamental equation of ellipsometry. We think, it is important to get a basic understanding of the fundamental equation. The derivation follows [11] pp. 529 - 531.

The plane wave components for incident light can be written in field components as:

$$E_p = E_{0_p} e^{ia_p} \tag{5}$$
$$E_s = E_{0_s} e^{ia_s} \tag{6}$$

The same reasoning holds for the reflected plane wave

$$R_p = R_{0_p} e^{ib_p} \tag{7}$$
$$R_s = R_{0_s} e^{ib_s} . \tag{8}$$

The reflection process is considered as a combination of an attenuation and a phase shift. Therefore two variables ρ_p, ρ_s are introduced with

$$R_p = \rho_p E_p \tag{9}$$
$$R_s = \rho_s E_s . \tag{10}$$

Substituting, we get

$$\rho = \frac{\rho_p}{\rho_s} \frac{R_{0_p}/E_{0_p}}{R_{0_s}/E_{0_s}} e^{i(b-a)} \tag{11}$$

with $a = a_p - a_s$ and $b = b_p - b_s$. Finally, we write the equation in terms of attenuation and phase

$$\rho = tan\Psi e^{i(\Delta)} \tag{12}$$

with attenuation $tan\Psi = \frac{R_{0_p}/E_{0_p}}{R_{0_s}/E_{0_s}}$ and phase $\Delta = b - a$.

Appendix - Physically plausible BRDFs and Microfacets

BRDFs are considered physically plausible if they are based on valid assumptions of the physical structure of surfaces. The most prominent model is the Torrance-Sparrow model. Most physically plausible BRDFs base on the theory of microfacets, i.e. a surface

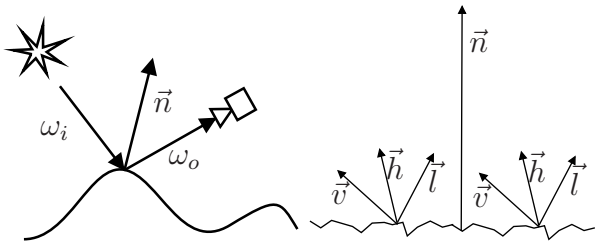

Fig. 10: The bidirectional reflectance function (BRDF) is defined by the ratio of emitted radiance to irradiance for a given incident angle (ω_i) and exitant angle (ω_o) w.r.t. the surface normal (left). Physically plausible BRDFs, e.g. the Torrance-Sparrow model, base on valid assumptions of the physical structure of surfaces. This includes the concept of microfacets, which reflect light from an incoming direction $\vec{l}$ to an outgoing direction $\vec{v}$. Their surface normal then is the halfway-vector $\vec{h}$. The overall amount of microfacets with normal $\vec{h}$ on a surface with normal $\vec{n}$ is defined by the distribution function D (right).

patch is made of many optically flat microfacets with varying facet normal orientation. Some microfacets block the light transport for certain incident and exitant angles, e.g. by shadowing or masking. Thus, such a BRDF consists of a geometry term G that models the shadowing and masking, a Fresnel-Term F for the fraction of light reflected from an optically flat microfacet and a distribution term D to model the distribution of microfacets with a certain normal orientation distribution. This term is most important, as it defines the brightness, size, and shape of the specular highlight, Fig. 10 (right).

We fitted the Fresnel-terms with the parameters n (refractive index) and k (extinction coefficient) and the following distribution terms D for their parameter β:

- Blinn-Phong [5]
  $D = cos\angle(\vec{h},\vec{n})^{\frac{-log(2)}{log(cos(\beta))}}$
  with β the exponential parameter.
- Gaussian [13]
  $D = exp(-(\frac{\sqrt{log(2)}}{\beta}cos(\angle(\vec{h},\vec{n}))^2))$,
  i.e. the facets are Gaussian distributed. It specifies the amount of facets oriented at an angle $\frac{\angle(\vec{h},\vec{n})}{\beta}$ from the average surface normal.
- Beckmann [14]
  $D = \frac{1}{\beta^2 cos(\angle(\vec{h},\vec{n}))^4}exp(-(tan(\angle(\vec{h},\vec{n}))/\beta)^2))$,
  where β is the RMS slope of the surface microfacets (the surface roughness)
- Trowbridge and Reitz [15], where microfacets are modeled as ellipsoids with eccentricity c:
  $D = (\frac{c^2}{\angle(\vec{h},\vec{n})^2\cdot(c^2-1)+1})^2$,
  $c = \sqrt{\frac{cos(\beta)^2-1}{cos(\beta)^2-\sqrt{2}}}$ describes the ratio of the lengths of the two main axes.

Note, that $\vec{n}$ and $\vec{h}$ refer to the surface normal and microfacet normal, i.e. the halfway-vector incident $\vec{l}$ and exitant $\vec{v}$ ray, Fig. 10 (right). Exemplary fitting results are shown in Tab 1.

Appendix - Predictive Rendering

While the most common Believable Rendering aims at conveying an impression of a scene to the viewer, Predictive Rendering has the goal to simulate the light transport in the scene and thus predict the effect of a virtual scene with real-world properties on an image captured with a camera placed inside that scene. This brings great advantages for applications where the appearance of objects or a scene is critical, e.g. in architecture, gemstone prototyping, or the automotive industry; as it provides imaging accuracy.

Typical current research areas in the Predictive Rendering are Scene modeling, Spectral Rendering, unbiased Image Synthesis, Error analysis on the rendering pipeline, and accuracy Verification. Our article integrates into the Predictive Rendering pipeline because it verifies the physical accuracy of BRDF models that are currently used.

6 Acknowledgements

The authors would like to thank the anonymous reviewers for their comments. The ellipsometric measurements were conducted at the Inst. f. Angewandte Physik, TU Braunschweig under supervision of PD Dr. Uwe Rossow and Prof. Dr. Hangleiter. The coins were provided bei Muenzhandelsgesellschaft Deutsche Muenze, Braunschweig.

7 Author Biography

Kai Berger
PhD student at Computer Graphics Lab at TU Braunschweig, Germany.
Studied Computer Science at TU Braunschweig, Germany.
Diploma (2008) in Computer Science, TU Braunschweig, Germany.
ACM, IEEE member
Interests: Predictive Rendering, Capturing Natural Phenomena

Andrea Weidlich
Technical Artist at Realtime Technology AG in Munich, Germany and External Lecturer at Vienna University of Technology.
Studied Computer Science and Computer Science Management at Vienna University of Technology, Austria.
MA (2011) in Applied Media, University for Applied Arts Vienna, Austria. MSc (2005) in computer science and a MSc in computer science management, Vienna University of Technology, Austria.
PhD (2009) in computer science Vienna University of

Fresnel terms						
	Copper ($\lambda = 516nm$)	Galvanized Steel ($\lambda = 500nm$)	Steel ($\lambda = 500nm$)	Aluminum Foil ($\lambda = 516nm$)	Gold ($\lambda = 516nm$)	Silver ($\lambda = 495nm$)
n	1.030	3.708	2.400	0.875	0.549	0.29
k	2.460	4.721	3.699	6.233	1.810	3.04
Torrance-Sparrow BRDF with Blinn-Phong microfacet distribution						
	Copper ($\lambda = 516nm$)	Galvanized Steel ($\lambda = 500nm$)	Steel ($\lambda = 500nm$)	Aluminum Foil ($\lambda = 516nm$)	Gold ($\lambda = 516nm$)	Silver ($\lambda = 495nm$)
n	1.032	3.708	2.400	0.875	0.549	0.289
k	2.459	4.721	3.700	6.233	1.810	3.040
β	0.786	0.867	0.255	0.637	0.443	0.793
Torrance-Sparrow BRDF with Gaussian microfacet distribution						
	Copper ($\lambda = 516nm$)	Galvanized Steel ($\lambda = 500nm$)	Steel ($\lambda = 500nm$)	Aluminum Foil ($\lambda = 516nm$)	Gold ($\lambda = 516nm$)	Silver ($\lambda = 495nm$)
n	1.232	3.708	2.471	0.876	0.55	0.289
k	2.458	4.721	3.500	6.233	1.81	3.04
β	0.358	0.213	0.307	0.438	0.218	0.825
Torrance-Sparrow BRDF with Beckmann microfacet distribution						
	Copper ($\lambda = 516nm$)	Galvanized Steel ($\lambda = 500nm$)	Steel ($\lambda = 500nm$)	Aluminum Foil ($\lambda = 516nm$)	Gold ($\lambda = 516nm$)	Silver ($\lambda = 495nm$)
n	1.032	3.708	2.400	0.875	0.549	0.289
k	2.459	4.721	3.700	6.233	1.810	3.04
β	0.786	0.867	1.180	0.637	0.866	0.793
Torrance-Sparrow BRDF with Trowbridge and Reitz microfacet distribution						
	Copper ($\lambda = 516nm$)	Galvanized Steel ($\lambda = 500nm$)	Steel ($\lambda = 500nm$)	Aluminum Foil ($\lambda = 516nm$)	Gold ($\lambda = 516nm$)	Silver ($\lambda = 495nm$)
n	1.232	3.708	2.471	0.875	0.55	0.289
k	2.458	4.721	3.500	6.233	1.81	3.040
β	0.187	0.259	0.246	0.501	0.185	0.736

TABLE 1: We fitted the Fresnel terms and Torrance-Sparrow BRDF with different microfacet distributions for $\lambda = 516nm$ (Copper, Aluminum, Gold), $\lambda = 495nm$ (Silver) and $\lambda = 500nm$ (Steel, Galvanized Steel) using Mathematica's *NonLinearModelFit*. The parameter n is the refractive index, k is the extinction coefficient, and β models the microfacet distribution's surface roughness. For each material we provided the initial guess for n, k from the literature [12].

Technology, Austria.
Interests: Predictive rendering with a special focus on gemstone prototyping and appearance modeling.

Alexander Wilkie
Associate Professor at Charles University in Prague, Czech Republic, since 2008
Studied Computer Science at Vienna University of Technology, Austria.
PhD (2001) in Computer Science, Vienna University of Technology.
Habilitation (2008) in Applied Computer Science, Vienna University of Technology.
ACM SIGGRAPH, IEEE member.
Interests: Predictive Rendering, Colour Science.

Marcus Magnor Full professor and head of the Computer Graphics Lab at TU Braunschweig Studied Physics at Würzburg University and the University of New Mexico, respectively.
BA (1995) and MSc (1997) in Physics, Würzburg University.
PhD (2000) in Electrical Engineering, Erlangen University.
Established the Independent Research Group Graphics-Optics-Vision at the Max-Planck-Institut Informatik in Saarbrücken (2002).
Habilitation in 2005 and venia legendi for Computer Science, Saarland University.
Fulbright Scholar (2009) at the University of New Mexico, USA as Adjunct Professor at the Physics and Astronomy Department.
ACM SIGGRAPH, IEEE fellow
Interests: visual computing, i.e. visual information processing from image formation, acquisition, and analysis to image synthesis, display, perception, and cognition. Areas of research include, but are not limited to, computer graphics, computer vision, visual perception, image processing, computational photography, astrophysics, imaging, optics, visual analytics, and visualization.

REFERENCES

[1] B. T. Phong, "Illumination for Computer Generated Pictures," *Comm. ACM*, vol. 18, no. 6, pp. 311–317, 1975.
[2] K. E. Torrance and E. M. Sparrow, "Theory for Off-Specular Reflection from Roughened Surfaces," *JOSA*, vol. 57, no. 9, pp. 1105–1114, 1967.
[3] G. J. Ward, "Measuring and Modeling Anisotropic Reflection," in *Proc. of SIGGRAPH*, 1992, pp. 265–272.
[4] W. Matusik, H. Pfister, M. Brand, and L. McMillan, "A Data-Driven Reflectance Model," *Transactions on Graphics*, vol. 22, no. 3, pp. 759–769, 2003.
[5] J. F. Blinn, "Models of Light Reflection for Computer Synthesized Pictures," in *Proc. of SIGGRAPH*, 1977, pp. 192–198.
[6] R. L. Cook and K. E. Torrance, "A Reflectance Model for Computer Graphics," in *Proc. of SIGGRAPH*, 1981, pp. 307–316.

[7] A. Ghosh, T. Chen, P. Peers, C. Wilson, and P. Debevec, "Circularly polarized spherical illumination reflectometry," in *ACM Transactions on Graphics (TOG)*, vol. 29, no. 6. ACM, 2010, p. 162.
[8] P. Callet *et al.*, "Virtual restoration of bronze-3d capture and optical simulation in parallel spectral ray-tracing," in *International Cultural Heritage Informatics Meeting ICHIM*. Citeseer, 2005.
[9] P. Callet, F. De Contencin, A. Zymla, P. Denizet, T. Hilpert, K. Miyazawa, and B. Robin, "An emblematic bronze from cyprus the idalion project," *Digital Heritage*, pp. 206–224, 2010.
[10] W. Matusik, H. Pfister, L. McMillan, and M. Brand, "MIT/Merl BRDF Database (2003) http://graphics. csail. mit. edu/˜ wojciech."
[11] D. Goldstein and E. Collett, *Polarized light*. CRC, 2003.
[12] E. D. Palik, *Handbook of Optical Constants of Solids*. Academic Press, 1985.
[13] K. Torrance and E. Sparrow, "Theory for off-specular reflection from roughened surfaces," *J. Optical Soc. America*, vol. 57, pp. 1105–1114, 1967.
[14] P. Beckmann and A. Spizzichino, *The Scattering of Electromagnetic Waves from Rough Surfaces*. Pergamon Press, 1963.
[15] T. Trowbridge and K. Reitz, "Average irregularity representation of a rough surface for ray reflection," *JOSA*, vol. 65, no. 5, pp. 531–536, 1975.
[16] M. Pharr and G. Humphreys, *Physically based rendering: From theory to implementation*. Morgan Kaufmann, 2004.
[17] F. Durand and J. Dorsey, "Fast bilateral filtering for the display of high-dynamic-range images," in *ACM Transactions on Graphics (TOG)*, vol. 21, no. 3. ACM, 2002, pp. 257–266.